Neuron
Article

Selective Disruption of One Cartesian Axis of Cortical Maps and Receptive Fields by Deficiency in Ephrin-As and Structured Activity

Jianhua Cang,[1,3,4] Cristopher M. Niell,[1,4] Xiaorong Liu,[3] Cory Pfeiffenberger,[2] David A. Feldheim,[2,*] and Michael P. Stryker[1,*]
[1]W.M. Keck Foundation Center for Integrative Neuroscience, Department of Physiology, University of California, San Francisco, San Francisco, CA 94143–0444, USA
[2]Department of Molecular, Cell, and Developmental Biology, University of California, Santa Cruz, Santa Cruz, CA 95064, USA
[3]Department of Neurobiology and Physiology, Northwestern University, Evanston, IL 60208, USA
[4]These authors contributed equally to this work.
*Correspondence: feldheim@biology.ucsc.edu (D.A.F.), stryker@phy.ucsf.edu (M.P.S.)
DOI 10.1016/j.neuron.2007.12.025

SUMMARY

The topographic representation of visual space is preserved from retina to thalamus to cortex. We have previously shown that precise mapping of thalamocortical projections requires both molecular cues and structured retinal activity. To probe the interaction between these two mechanisms, we studied mice deficient in both ephrin-As and retinal waves. Functional and anatomical cortical maps in these mice were nearly abolished along the nasotemporal (azimuth) axis of the visual space. Both the structure of single-cell receptive fields and large-scale topography were severely distorted. These results demonstrate that ephrin-As and structured neuronal activity are two distinct pathways that mediate map formation in the visual cortex and together account almost completely for the formation of the azimuth map. Despite the dramatic disruption of azimuthal topography, the dorsoventral (elevation) map was relatively normal, indicating that the two axes of the cortical map are organized by separate mechanisms.

INTRODUCTION

Most sensory projections in the brain are mapped topographically, such that the spatial organization of stimulus representation is maintained throughout successive stages of processing (Chklovskii and Koulakov, 2004; McLaughlin and O'Leary, 2005). In the visual system, for example, neighboring neurons in the retina project their axons to neighboring neurons in the dorsal lateral geniculate nucleus (dLGN), which, in turn, project to neighboring targets in the primary visual cortex (V1), thus preserving a continuous retinotopic representation of the visual world. Both molecular guidance cues and patterned neuronal activity are important for the establishment of the topographic maps (Flanagan, 2006; McLaughlin and O'Leary, 2005; Torborg and Feller, 2005). EphAs and ephrin-As are cell-surface-bound axon guidance molecules that are expressed in gradients in each visual area and are required for the development of topographic maps throughout the visual system (Flanagan and Vanderhaeghen, 1998; O'Leary and Wilkinson, 1999). In mice deficient for ephrin-A2, -A3, and -A5 (ephrin-A triple KOs), the anatomical and functional maps of geniculocortical projections are disrupted specifically along the nasotemporal (azimuth) axis (Cang et al., 2005a).

Another source of positional information comes from correlated bursts of spontaneous activity that propagate as waves across the retina early in development, which carry information about nearest neighbors in their correlation structure (Torborg and Feller, 2005; Wong, 1999). In the first postnatal week, these waves depend on cholinergic activity for their propagation, while later they become driven by glutamatergic transmission (Torborg and Feller, 2005; Wong, 1999). Retinogeniculate and geniculocortical mapping along the azimuth axis is imprecise when these early waves are disrupted pharmacologically or genetically (due to deletion of the β2 subunit of the nicotinic acetylcholine receptor) (Cang et al., 2005b). This indicates that structured activity from the retina, transferred to the dLGN and visual cortex, is also used to instruct the formation of geniculocortical maps. However, although topography is not normal in either ephrin-A or β2 mutants, each retains a rough map along the azimuth axis (Cang et al., 2005a, 2005b).

Taken together, these two studies raise important questions about the interaction between neuronal activity and ephrin-A signaling and their roles in mapping geniculocortical projections. First, do ephrin-A- and activity-dependent mechanisms act in series in the formation of cortical maps? In support of this possibility, it has been shown that, in spinal motor neurons, normal patterns of spontaneous activity are required for the expression of specific guidance molecules, including EphA4, a receptor for ephrin-A2, -A3, and -A5 (Hanson and Landmesser, 2004). It has also been shown in vitro that the blockade of neural activity inhibits the ability of ephrin-A5 to act as an axon repellent (Nicol et al., 2007). These results suggest that EphA/ephrin-A signaling might act downstream of neural activity to generate topographic maps. Conversely, ephrin-A signaling might act upstream of neural activity if deletion of ephrin-As in the retina led to altered

neural activity patterns that produced a disrupted geniculocortical map. Although it has been shown that the ephrin-A triple KOs have propagating retinal waves similar to those in the wild-type (Pfeiffenberger et al., 2005), it remains possible that transmission of these waves of activity to the visual cortex could be disrupted in the ephrin-A triple KOs. Alternatively, ephrin-A signaling and structured neuronal activity could be separate pathways with distinct actions, though they might also interact. For example, EphA/ephrin-A signaling may act to form "rough" topography, while neural activity acts in clustering correlated inputs to promote fine-scale topography (Cline, 2003).

Do these mechanisms, and the maps they generate, play a role in the establishment of connectivity to individual cortical cells, which results in structured receptive fields? Because previous studies have used anatomy and large-scale mapping to measure topography, it is unknown whether the receptive fields of individual neurons are spatially distorted or structured normally but respond to inappropriate regions of visual space in the absence of these mechanisms.

In this study, we seek to answer these questions by examining functionally and anatomically the cortical maps of mice deficient in both ephrin-As and early retinal waves. We find that in these mice the topography of geniculocortical projections is almost abolished along the azimuth axis, resulting in a severe disruption of functional retinotopic maps in the cortex. We also find that the spatial structure of individual cortical receptive fields in these mice is disrupted, again selectively along the azimuth axis. In contrast, the receptive fields of neurons in the dLGN were mostly normal in size and shape, but were abnormally scattered along the azimuthal axis, though not sufficiently so to account for the cortical mapping defect. Importantly, the functional and anatomical mapping defects in these combination knockouts are much more severe than in mice lacking either ephrin-As or retinal waves. These results establish that ephrin-As and patterned neuronal activity are distinct pathways that mediate map formation in the visual cortex and that together they largely account for the formation of the azimuth map. We also show that these two pathways act together in the establishment of individual receptive fields and cell-specific connectivity. Finally, we find that a relatively normal elevation map is preserved in the cortex of these combination knockouts, despite the near abolition of the azimuth map, revealing that the two Cartesian axes of the cortical map are organized by independent mechanisms.

RESULTS

To determine the consequences for cortical retinotopic maps and receptive fields of simultaneously removing ephrin-As and disrupting early retinal waves, mice lacking the β2 subunit of the nicotinic acetylcholine receptor ($\beta2^{-/-}$) (Cang et al., 2005b; Xu et al., 1999) were crossed with those deficient for ephrin-As (Cang et al., 2005a; Feldheim et al., 2000; Pfeiffenberger et al., 2005) to obtain ephrin-A2A5-β2 combination KOs ($A2^{-/-}/A5^{-/-}$-$\beta2^{-/-}$) (Pfeiffenberger et al., 2006). Because ephrin-A3 and β2 are genetically linked, we were unable to create an ephrin-A2/A3/A5-β2 quadruple KO. In the following sections, we present results from our imaging, anatomical, and physiological studies to characterize cortical retinotopic maps and RFs in the ephrin-A2A5-β2 combination KOs. Their littermates and additional mice with the same genetic background were used as controls, including $A2^{-/-}/A5^{-/-}$-$\beta2^{+/\pm}$ and $A2^{+/\pm}/A5^{+/-}$-$\beta2^{-/-}$. Although the $\beta2^{-/-}$ mice lack nictonic acetylcholine receptors ubiquitously, retinal application of epibatidine, which disrupts retinal waves but does not eliminate spontaneous activity, mimics the $\beta2^{-/-}$ phenotype (Cang et al., 2005b; Chandrasekaran et al., 2005; Pfeiffenberger et al., 2005), suggesting that β2 action is due to its requirement in the retina. Likewise, although ephrin-As are expressed throughout the visual pathway, misexpression in the cortex alone has been shown to result in mapping abnormalities (Cang et al., 2005a).

Functional Cortical Maps in Ephrin-A2A5-β2 Combination KOs

We first determined the functional maps of cortical retinotopy by optical imaging of intrinsic signals from ephrin-A2A5-β2 KOs and their littermate controls. Adult mice between 2 and 6 months old were anesthetized and presented with thin bars drifting continuously and periodically across a video monitor while we imaged the posterior cortex. The reflectance signals were analyzed using the temporally encoded mapping paradigm (Cang et al., 2005a, 2005b; Kalatsky and Stryker, 2003) to generate maps of the topographic organization of V1.

In the control mice, both ephrin-$A2^{-/-}/A5^{-/-}$-$\beta2^{+/-}$ and ephrin-$A2^{+/-}/A5^{+/-}$-$\beta2^{-/-}$, the gross polarity of the azimuth map in V1 persisted (Figures 1A and 1B). In contrast, in the ephrin-A2A5-β2 combination KOs, the smooth progression of visual field location in the visual cortex was absent (Figure 1C and see Figure S1 available online). These observations were confirmed by quantitative analysis of map quality (Cang et al., 2005a, 2005b). The cortical maps of ephrin-A2A5-β2 combination KOs were much more scattered than those of their controls (Figure 1D; map scatter: 30.3° ± 2.5° for combination KOs, n = 10; 9.4° ± 2.7° for $A2^{-/-}/A5^{-/-}$-$\beta2^{+/-}$, n = 5; and 12.8° ± 3.9° for $A2^{+/\pm}/A5^{+/-}$-$\beta2^{-/-}$, n = 4; $p < 0.001$, one-way ANOVA, and $p < 0.01$ between combination KOs and the controls), indicating a much more severe disruption of cortical maps in mice deficient in both ephrin-A signaling and early retinal waves. The defect of azimuth maps is also obvious in the response amplitude (combination KOs: 0.69 ± 0.05 × 10^{-4} fractional change in reflection, n = 10; $A2^{-/-}/A5^{-/-}$-$\beta2^{+/\pm}$: 1.16 ± 0.16, n = 6; $A2^{+/\pm}/A5^{+/-}$-$\beta2^{-/-}$: 1.00 ± 0.18, n = 3; $p < 0.05$).

Remarkably, despite the severe disruption of azimuth maps in combination KOs, the elevation maps were relatively normal, comparable to those of their littermate controls in terms of map scatter (Figures 1E–1H, p = 0.70, one-way ANOVA) and response amplitude (combination KOs: 1.66 ± 0.18; $A2^{-/-}/A5^{-/-}$-$\beta2^{+/-}$: 1.72 ± 0.17; $A2^{+/\pm}/A5^{+/-}$-$\beta2^{-/-}$: 1.67 ± 0.52; p = 0.98). This finding indicates that the mechanisms of topographic mapping of the two axes are unlinked.

Cortical Maps Revealed by Spatially Restricted Stimuli

The absence of a phase progression and weak response amplitude in the azimuth map of the ephrin-A2A5-β2 combination KO (Figure 1C) suggests a severe and specific disruption of topography along the nasotemporal axis in the primary visual cortex. However, such a result could also be due to a lack of response

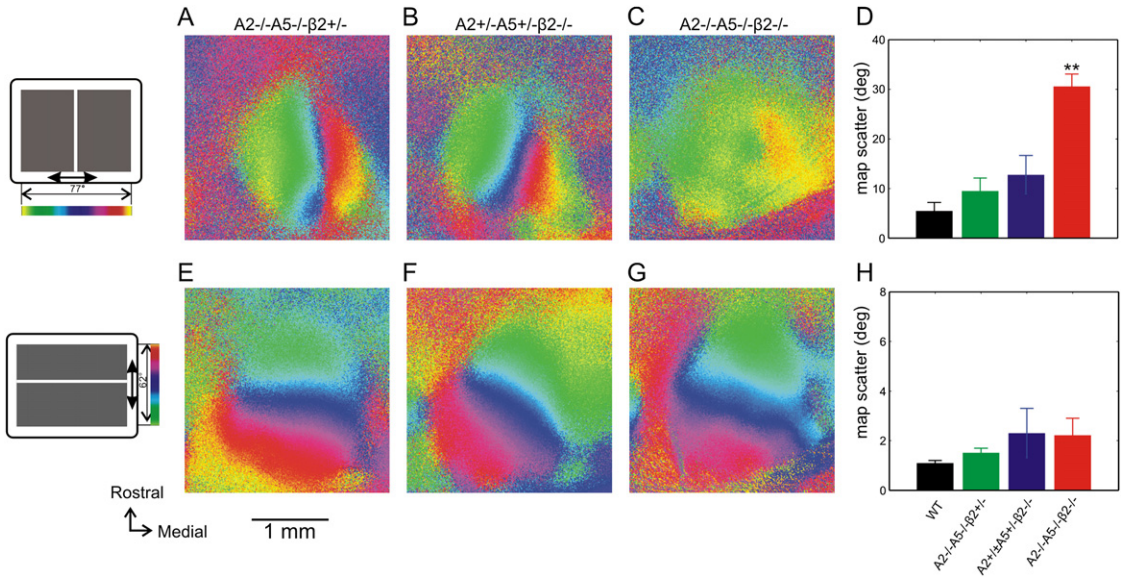

Figure 1. Cortical Azimuth Maps Are Severely Disrupted in Ephrin-A2A5-β2 Combination KOs

(A–C) Cortical azimuth maps of an $A2^{-/-}A5^{-/-}\beta2^{+/-}$ (A), an $A2^{+/-}A5^{+/-}\beta2^{-/-}$ (B), and an $A2^{-/-}A5^{-/-}\beta2^{-/-}$ combination KO (C). The color code used to represent positions of different azimuthal lines on the stimulus monitor is shown to the left of panel (A). Note that the lack of retinotopic organization in the map of $A2^{-/-}A5^{-/-}\beta2^{-/-}$ combination KO.

(D) Quantification of map scatters for the azimuth maps of these genotypes.

(E–H) Elevation maps of the same three mice and quantification of their map scatter. The color code is shown to the left.

Error bars represent SEM.

of cortical neurons to the drifting vertical bars used in our imaging experiments. To resolve this issue, we took advantage of the fact that the combination KOs and their controls have relatively normal elevation maps and thus respond well to drifting horizontal bars (Figures 1E–1G). We used short horizontal bars drifting vertically to define the area of activation in the cortex. Maps of response magnitude to such spatially restricted stimuli are shown in grayscale in Figures 2A–2C. In the ephrin-$A2^{-/-}$/$A5^{-/-}$-$\beta2^{+/-}$ mouse, the response area in V1 was spatially confined (Figure 2a) along the iso-azimuth area as predicted from the full-screen azimuth map, similar to that in the wild-type mouse (WT, data not shown, and also see Kalatsky and Stryker [2003]). In the mice with disrupted retinal waves, e.g., $A2^{+/-}$/$A5^{+/-}$-$\beta2^{-/-}$, the response area was a bit more diffuse (Figure 2B), consistent with the mapping error of geniculocortical projections we observed previously using imaging with full-screen stimuli and anatomical and physiological methods (Cang et al., 2005b). In comparison, the spatially restricted stimulus activated a much larger area in the visual cortex of ephrin-A2A5-β2 combination KO (Figure 2C), spanning much of the entire V1. In order to quantify the above observations on these spatially encoded maps, we determined the size of the response area to the restricted stimulus and calculated its ratio to that of the full elevation map (Figure 2D). The ratio was 38% ± 4.5% in WTs (n = 4), 51% ± 11.8% in ephrin-$A2^{-/-}$/$A5^{-/-}$-$\beta2^{+/-}$ (n = 3), and 54% ± 3.7% in the $A2^{+/\pm}$/$A5^{+/-}$-$\beta2^{-/-}$, while it was much greater in the combination KOs (72% ± 6.9%, n = 6; $p < 0.05$, n = 4, between combination KO and the controls), confirming a severe disruption of cortical maps in these mice deficient for both ephrin-A signaling and early retinal waves.

We further sought to determine whether any functional organization in azimuth remained in these combination KOs by imaging cortical responses to restricted stimuli at different locations (Figures 2E–2H and Figures S2 and S3). As the center of the short bar was shifted horizontally in the visual field, the area of activation in the visual cortex moved along the azimuth axis of the retinotopic maps in the control mice (Figure S2). We displayed the maps obtained with such spatially restricted stimuli. The color of each pixel is determined by the relative response magnitude evoked by the bars along the three positions. In WT and heterozygous controls, clear color progression is seen (Figures 2E and 2F and Figure S3). In the combination KOs, the color progression is disrupted (Figures 2G and 2H and Figure S3), as the response area to each position was much larger, as described above. Notably, an overall polarity of the color progression could still be detected according to the center positions of the stimulus (Figures 2G and 2H), indicating that the combination KOs still have a remnant, albeit severely disrupted, azimuth map in their visual cortex.

Geniculocortical Maps in Ephrin-A2A5-β2 Combination KOs

To determine the anatomical basis of the severe disruption of cortical azimuth maps in the ephrin-A2A5-β2 combination KOs, we examined the projection patterns from dLGN to V1 by injecting the retrograde marker cholera toxin subunit B (CTB) into V1 to retrogradely label dLGN neurons. In WTs, these injections label a column of cell bodies in the geniculate (Cang et al., 2005b). In coronal sections of the dLGN, neurons labeled by injecting two colors of tracers about 500 μm apart formed distinct clusters. When the two tracers were injected at sites separated along

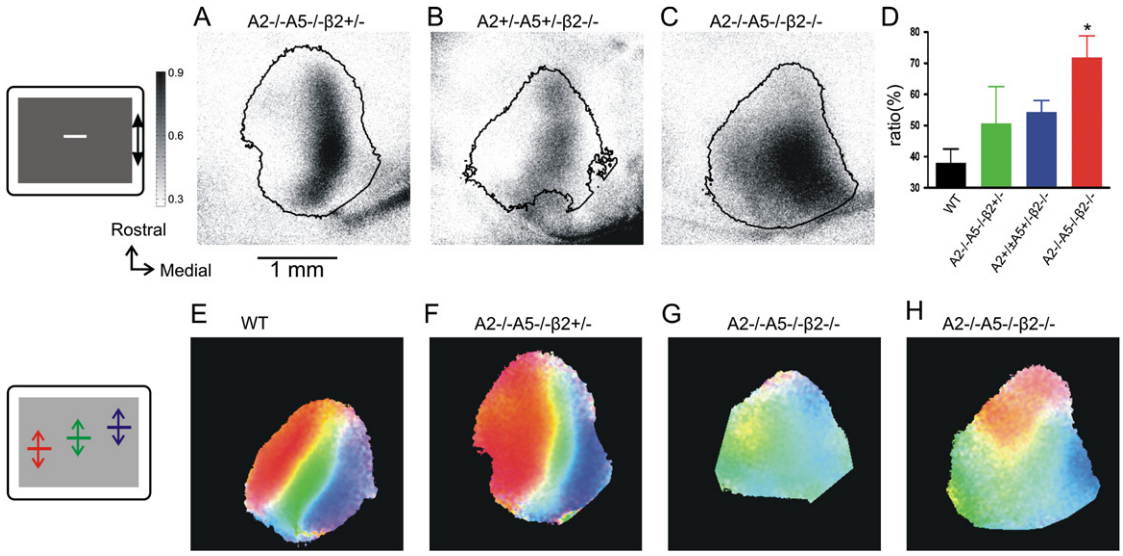

Figure 2. Cortical Maps Revealed by Spatially Restricted Stimuli

(A–C) Maps of response magnitude of an $A2^{-/-}A5^{-/-}\beta2^{+/-}$ (A), an $A2^{+/-}A5^{+/-}\beta2^{-/-}$ (B), and an $A2^{-/-}A5^{-/-}\beta2^{-/-}$ combination KO (C) to a spatially restricted stimulus as diagrammed in the leftmost panel. The response magnitude is displayed as fractional change in reflection $\times 10^4$ in grayscale, shown to the left of panel (A). The black contour on each panel circles the region activated by full-screen stimulus (thresholded at a level of 30% of the peak response).

(D) Activated areas in response to the spatially restricted stimulus as a percentage of full-screen elevation maps for different genotypes.

(E–H) Topographic maps determined by spatially restricted stimuli. A diagram illustrating spatially restricted stimuli used to assay azimuth maps is shown in the leftmost panel. The color of each pixel on the map is determined by the relative response magnitude evoked by the bars along the three positions, with color component according to the diagram. (E) WT, (F) heterozygous control, (G and H) two examples of combination knockouts showing the range of results. Error bars represent SEM.

the lateral-medial axis in the cortex (Figure 3A, corresponding to the representation of azimuth), clusters of retrogradely labeled cells were separated lateromedially in the dLGN in WT animals (Figure 3B). In combination KOs, the labeled cells overlapped completely in the dLGN (Figure 3D). When the tracer injection sites were separated rostrocaudally in cortex (corresponding to the representation of elevation, Figure 3F), the clusters of labeled cells were completely distinct in all genotypes examined (Figures 3G–3I). We calculated an index to quantify the overlap between the two colors of labeled pixels (see Experimental Procedures for details; Figure 3E and J). In the WTs, the overlap index was 0.39 ± 0.03 (mean ± SEM, n = 4) along the azimuth axis, while that of the ephrin-A2A5-β2 combination KOs was much greater (4.46 ± 0.99, n = 7; $p < 0.01$, one-way ANOVA; and $p < 0.05$ compared to WT, Newman-Keuls post-test). As a comparison, in ephrin-$A2^{-/-}$/$A5^{-/-}$-$\beta2^{+/-}$, the labeled cells of each color often still formed clusters with largely normal topography, with aberrant cells scattered in the dLGN and significant overlap of the two colors (Figure 3C). Correspondingly, the overlap index along the azimuth axis between the two colors (1.38 ± 0.48) was greater than in the WTs but significantly smaller than in the combination KOs ($p < 0.05$). We also used this method to analyze the tracing data in our previous studies. The overlap index was 0.98 ± 0.12 (n = 5) in the ephrin A2A3A5 triple KOs (Cang et al., 2005a) and 0.60 ± 0.08 (n = 5) for the β2 KOs (Cang et al., 2005b), confirming the defects we observed in those studies.

Previously, we did not systematically analyze the anatomical map along the elevation axis, although we did note that the labeled pixels in the β2 KOs were more spread out along the azimuth axis (Cang et al., 2005b). Here we found that the overlap index along the elevation axis was similarly small for all three genotypes (Figure 3J, $p > 0.05$). Similar results were observed when different thresholds were used to analyze the images. Together, these results demonstrate that the anatomical geniculocortical map in mice deficient for both ephrin-A signaling and early retinal waves is selectively disrupted along the azimuth axis.

Receptive Field Structure of Cortical Neurons in Ephrin-A2A5-β2 Combination KOs

A severely disrupted cortical map could reflect either of two possible scenarios of cortical RF organization. The RFs of individual cortical neurons could each have a normal spatial structure but not be organized topographically or the RFs of individual cortical neurons could be distorted spatially, with the distortion especially severe along the azimuth axis. To distinguish between these two possibilities, we studied the RF structures of cortical neurons with single-unit recording in the combination KOs using silicon microprobes with 16 sites aligned linearly to radially penetrate the layers of cortex. The RFs of cortical neurons were mapped with moving short bars, similar to those used in our imaging experiments. As in Figure 4, the spiking response of the recorded neuron is plotted against the position of the bar in the visual field in a color scale to illustrate its RF structure. The RFs of visually responsive units in WTs and controls were localized spatially, with an average radius of 15.7° ± 1.5° along the azimuth axis and 8.55° ± 0.6° in elevation (Figures 4C and 4D). In contrast, individual cortical RFs in the ephrin-A2A5-β2 combination KOs were selectively expanded by almost 2-fold along the azimuth

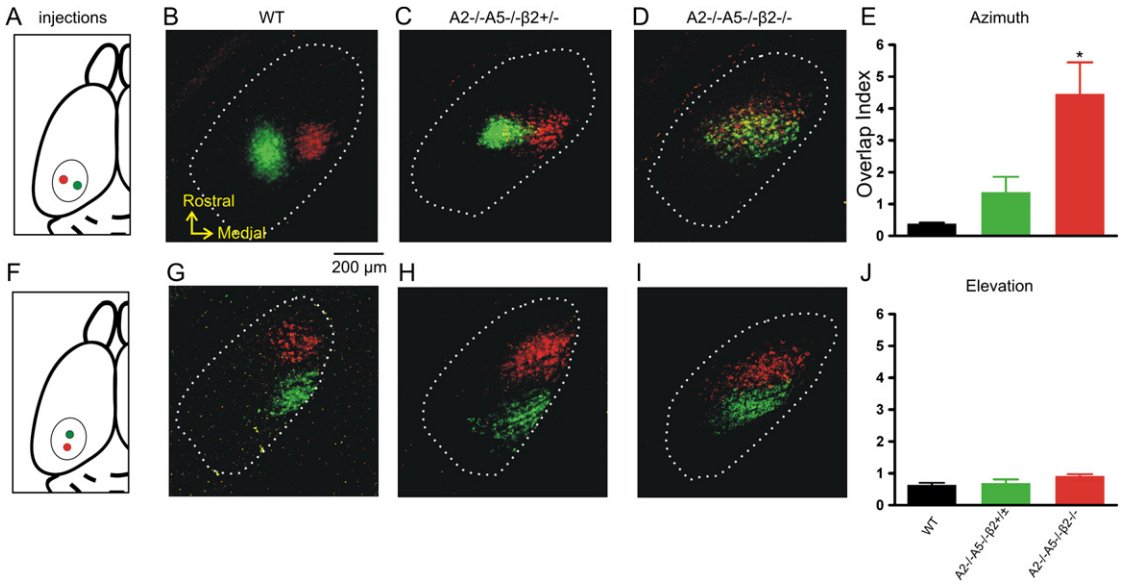

Figure 3. Disruption of Geniculocortical Map in Ephrin-A2A5-β2 Combination KOs

(A–D) Retrogradely labeled dLGN neurons of a WT (B), an $A2^{-/-}A5^{-/-}\beta2^{+/-}$ (C), and an $A2^{-/-}A5^{-/-}\beta2^{-/-}$ (D). Neurons were labeled by injections of CTB-Alexa 488 (green) and CTB-Alexa 568 (red) at 500 μm apart in V1 along lateromedial axis (A). In all the panels, dotted lines mark the border of dLGN. Note the overlap between the green and red cells in (D).

(E) Quantification of overlap between the two groups of labeled cells in the dLGN along the azimuth axis.

(F–J) Retrograde labeling and quantification for dLGN neurons when the tracers were injected along elevation axis.

Error bars represent SEM.

axis (radius = 26.1° ± 2.5°; $p < 0.001$). Many of the RFs in the combination KOs spanned horizontally across almost the whole video monitor (Figure 4B) and often included more than one peak in their RFs (Figure 4B2). We have never seen such neurons in WTs. The peak RF amplitude averaged across all single units was also decreased in the combination KOs, from 4.70 ± 0.83 to 2.28 ± 0.71 spikes/s ($p < 0.05$, n = 61 units control, n = 58 units combination KO). The fact that the increase in receptive field size is accompanied by a similar reduction in response amplitude is consistent with a homeostatic mechanism, as observed by Chandrasekaran et al. (2007) in the superior colliculus of $\beta2^{-/-}$ mice.

We next examined the topographic organization of the cortical RFs. Because the silicon microprobe was aligned to radially span the cortex, we were able to simultaneously record from a number of units at the same location on the cortical sheet, which in a normal map would correspond to the same position in visual space. In WTs and combination heterozygous controls,

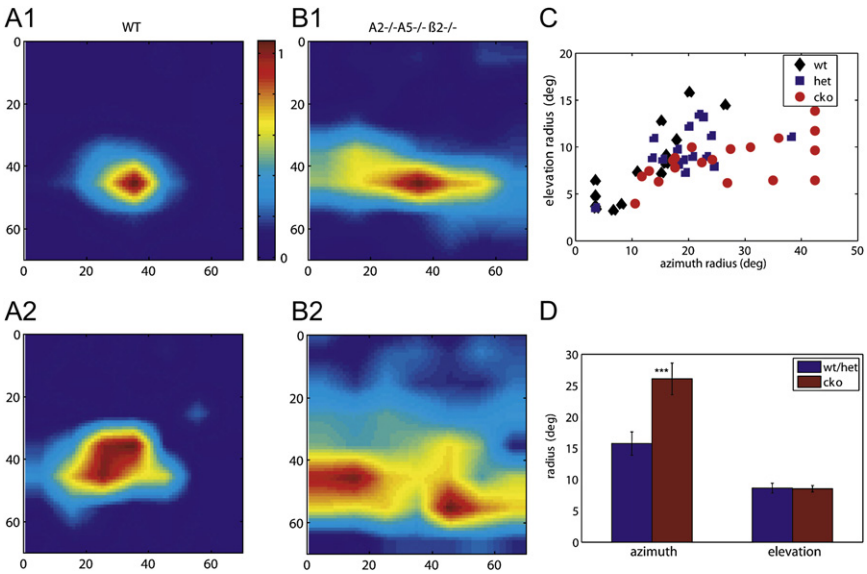

Figure 4. Single-Unit Recording in Visual Cortex Demonstrates that the Receptive Fields of Cortical Neurons in Combination KOs Are Selectively Enlarged in the Azimuthal Direction

(A and B) Representative receptive fields measured with moving short bars of two WT neurons (A1, 2) and two ephrin-A2A5-β2 combination KO neurons (B1, 2). Axes in degrees of visual space, color represents magnitude of response.

(C) Receptive field radii in degrees, by Gaussian fit to sweeping short bar data, for all single units recorded.

(D) Average receptive field size in azimuth and elevation from (C). (n = 31 units in control, 23 units combination KOs, from 5 animals each.)

Error bars represent SEM.

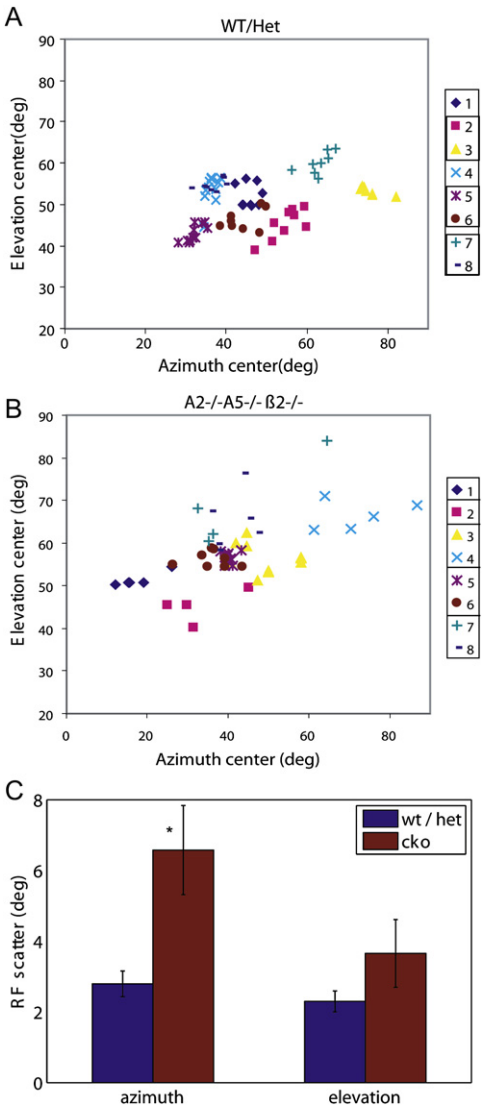

Figure 5. Topography Is Degraded, but Still Present, in Combination KOs

(A and B) Receptive field centers for multi-unit recordings for WT and heterozygous littermate controls (A) and combination KOs (B). Units from the same penetration site are shown with the same color and symbol. n = 8 penetrations from five animals each, four to ten simultaneously recorded multi-units per penetration.

(C) Scatter in receptive field center for all multi-units, relative to the mean of each penetration. n = 78 multi-units in controls, and n = 54 multi-units in combination knockouts (cko), from eight penetration in five animals each. Error bars represent SEM.

the RF centers of the multiunits from the same penetrations were clustered around the same locations in the visual field, with very small scatter along both azimuth and elevation axes (Figure 5A, azimuth = 2.8° ± 0.4°, elevation = 2.3° ± 0.3°). In the combination KOs, the scatter of RF centers was much greater than the in controls, especially in the azimuth direction (Figure 5B, azimuth = 6.5° ± 1.2°, $p < 0.05$; elevation = 3.7° ± 1.0°; n = 8 penetration sites, 5 animals each). However, the scatter did not span across the whole video monitor and instead the RFs of individual penetrations were centered around one location in the visual field, confirming that, despite the poor spatial restriction of individual receptive fields, a degraded topography with over 2-fold increase in scatter still persists in the visual cortex of these combination KOs.

Receptive Field Structure of Geniculate Neurons in Ephrin-A2A5-β2 Combination KOs

Previous studies on mice deficient in either structured activity or ephrin-A signaling have revealed anatomical mapping errors in both retinogeniculate and geniculocortical pathways. Recent anatomical experiments in the combination KOs revealed that the retinogeniculate map was much more abnormal than in either ephrin-A or β2 KOs alone (Pfeiffenberger et al., 2006). To assess the effect of this anatomical miswiring on individual receptive fields in dLGN and to determine how a disruption there could contribute to the functional deficits in cortex, we recorded from single units in dLGN. Traditional high-impedance tungsten electrodes were used to study RF structures using brief flashes of light and dark spots. As expected (Grubb and Thompson, 2003), dLGN neurons had spatially localized circular RFs in WTs (Figure 6A). In the combination KOs, in contrast to the finding in cortex, individual dLGN neurons generally had normal RFs (Figure 6B), although a small fraction showed enlargement in the azimuthal direction (Figures 6C and 6D, WT: 5.7° ± 0.3°, n = 35 units; combination KO: 7.3° ± 0.8°, $p < 0.01$, n = 38 units; 3 animals each). This lack of widespread disruption of individual RF size is consistent with the finding that the input to dLGN neurons is dominated by synapses from just one to three RGCs (Chen and Regehr, 2000; Jaubert-Miazza et al., 2005).

A disruption of local azimuthal topography was revealed by comparing the RF locations of units recorded simultaneously at the same site (Figure 6B). While RFs in the WT were clustered with an average scatter of just 2°, the average scatter was more than five times greater in the combination KOs (Figures 7A and 7C; WT: 2.0° ± 0.6°; combination KO: 11.8° ± 2.1°; $p < 0.001$, n = 20 sites each). As predicted by the anatomical projection (Pfeiffenberger et al., 2006), there was no difference between WT and KO in the topography of elevation (Figures 7B and 7C). Thus, in contrast to the cortex, dLGN cells in the combination KO generally maintain spatially restricted receptive fields, but their azimuthal positions are disrupted.

The observed defect in geniculate RFs raises the possibility that all of the RF disruption in cortex is simply inherited from the dLGN. To address this possibility, we generated a simple model for the pooling of geniculate input to create cortical RFs. This model treats geniculate RFs as Gaussians with the width and scatter measured in our single-unit recordings. We then assume that cortical RFs are formed by summing geniculate units over a sufficiently large region to generate the RF widths observed in WT mice. We allow the number of geniculate cells pooled to vary, since this number is still open to debate.

Figure 7D shows that this model (blue line) matches the observed WT cortical receptive field size (15.7°, dashed blue line) well when the number of geniculate inputs is more than about five. In contrast, using the geniculate RF properties from combination KOs (red line), including the dramatically increased

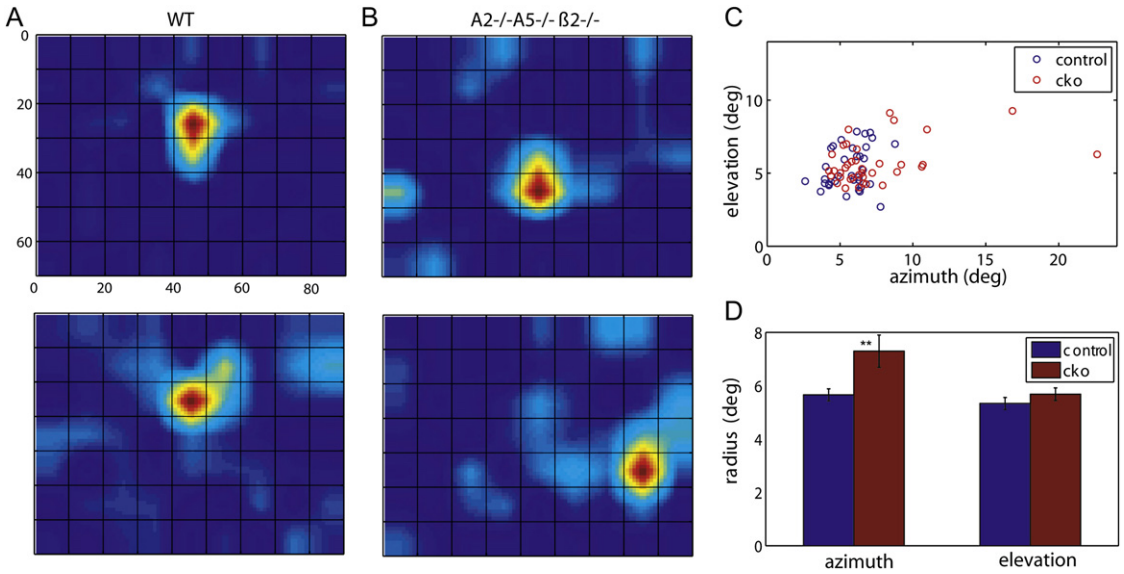

Figure 6. Single-Unit Receptive Fields in the dLGN

(A) Receptive fields of two single units recorded simultaneously in WT dLGN.

(B) Similar receptive fields in a combination KO are displaced in azimuth relative to each other.

(C) Scatter plot of single-unit receptive field radius shows normal receptive field size in combination KOs, except for a few units expanded in azimuth.

(D) Average receptive fields sizes (n = 35 units WT, 38 units combination KOs, 3 animals each).

Error bars represent SEM.

scatter, the model is far from accounting for the increased RF size in the cortex of combination KOs (26.1°, dashed green). Generating cortical RF sizes (green line) that match those observed in the combination KOs requires an additional 17° of scatter in the pooling of inputs to cortical neurons. Figure 7E shows the results from the same model for predictions of cortical map scatter. These results show the strong dependence of map scatter on the number of inputs being pooled—by summing a large number of dLGN receptive fields, the variance in the location of the centroid of the resulting cortical RFs is decreased. However, regardless of the number of inputs, the difference between cortical scatter predicted from WT dLGN (blue line) and combination KO dLGN (red line) is small. Adding in the additional 17° of post-LGN scatter needed to match the RF sizes (green line) predicts an increase in cortical RF scatter that makes it closer to our actual measurements (green dashed line). Both of these results suggest that the observed scatter in the dLGN is insufficient to explain the enlarged and mislocated cortical receptive fields seen in the combination KOs and therefore that geniculocortical and/or corticocortical connectivity are greatly disrupted.

DISCUSSION

In this study, we have investigated the interactions of patterned neuronal activity and ephrin-A signaling in the formation of cortical retinotopic maps. Our experiments demonstrate that the geniculocortical map is severely disrupted along the azimuth axis both anatomically and functionally in mice in which both ephrin-A2/A5 and early waves of spontaneous retinal activity are absent. We also found that the spatial structure of the cortical receptive fields in these mice is disrupted, selectively along the azimuth axis. The functional and anatomical mapping defects in these combination knockouts are strikingly more severe than in mice lacking either ephrin-As or retinal waves alone. Our results demonstrate that ephrin-A signaling and patterned neuronal activity, driven by the early retinal waves, together largely account for the formation of the azimuth map, as well as the structure of individual receptive fields. We also show that the functional azimuth and elevation maps are independent, with the nearly complete degradation of the former having negligible effect on the latter, supporting the notion of azimuth and elevation as the natural coordinate system of the visual pathway.

Molecular Cues and Structured Activity in Cortical Map Formation

Our recent studies had shown that both ephrin-As and early retinal waves are required for the formation of normal, precise retinotopic maps in the visual cortex (Cang et al., 2005a, 2005b). In mice deficient for either ephrin-As or early retinal waves, the anatomical and functional maps of geniculocortical projections are disrupted along the azimuth axis (Cang et al., 2005a). In both cases, scattered maps of low precision along this axis persist. These findings have been interpreted as supporting a model in which molecular cues, including EphA/ephrin-As, guide the formation of an initial coarse map of geniculocortical projections, and this coarse map is normally refined by correlated neuronal activity driven by retinal waves (Cang et al., 2005b; Cline, 2003; O'Leary and McLaughlin, 2005; Tsigankov and Koulakov, 2006). However, it remained possible before our current study that these two pathways are not independent in mapping

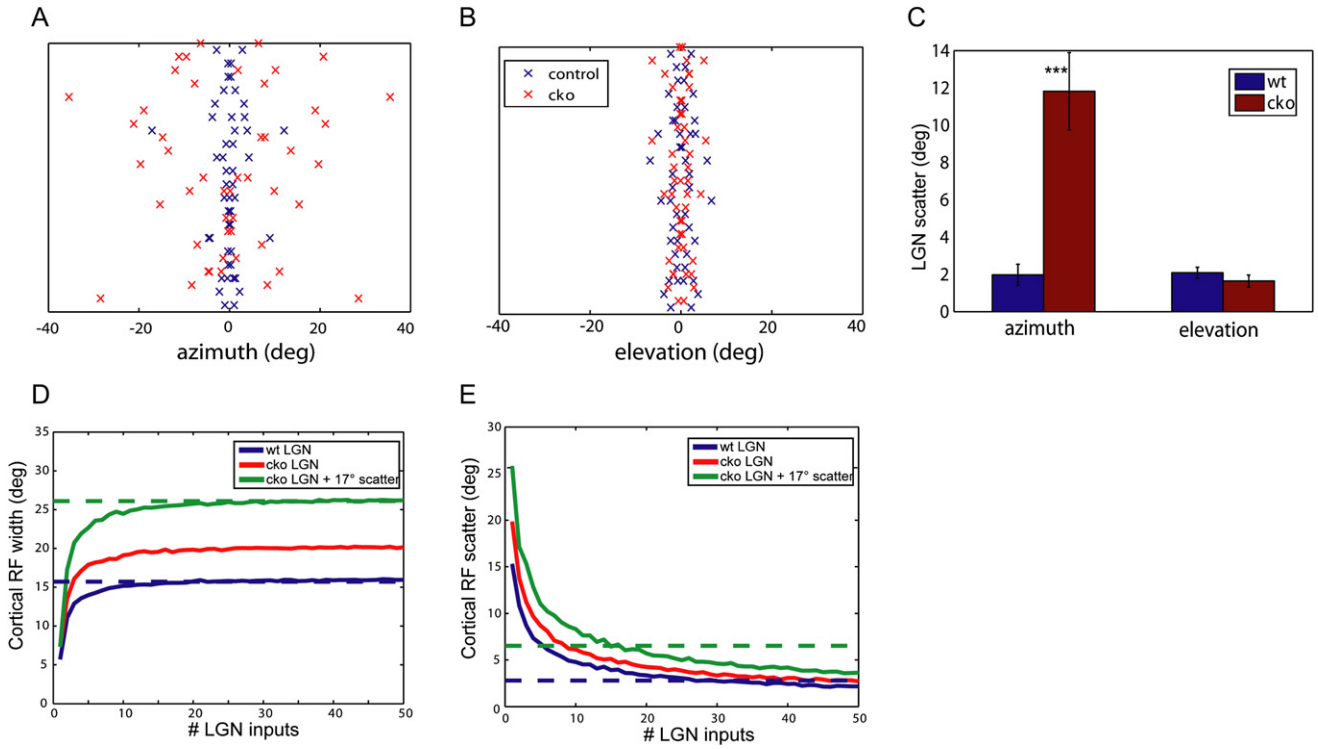

Figure 7. Disrupted Topography in dLGN, and Its Effect on Cortical Receptive Fields

(A) Position in azimuth of RF centers for single and multi-units recorded simultaneously in dLGN, aligned to the mean for that site.

(B) Position in elevation of receptive field centers.

(C) Average scatter in receptive field center for simultaneously recorded units (n = 20 sites, 3 animals each).

(D and E) Model of effects of dLGN receptive field parameters on cortical RF size (D) and RF scatter (E). Blue and green dashed lines demarcate observed cortical RF size in control and combination KO, respectively, while solid lines represent results of simulation with various geniculate RF parameters.

Error bars represent SEM.

geniculocortical projections. Some studies have suggested that neuronal activity may interact with EphA/ephrin-A signaling (Hanson and Landmesser, 2004; Nicol et al., 2007), and particularly, the recent finding that levels of activity in the visual system regulate ephrin-A responsiveness (Nicol et al., 2007) might be extrapolated to suggest that early retinal waves and ephrin-A act in a single linear pathway. The present study of ephrin-A2A5-β2 combination KOs provides a direct experimental test of this possibility in vivo. If patterned activity acts upstream of ephrin-As by modulating EphA/ephrin-A signaling, we would expect that combination KOs would have the same phenotype as ephrin-A mutants. Here we show that the combination KOs have dramatically stronger mapping defects than either ephrin-A2/A3/A5 triple KOs or β2 mutants. This is inconsistent with the idea that β2-dependent early retinal waves have their effect on cortical mapping solely via ephrin-As, or vice-versa, although it leaves open the possibility of other interactions between retinal waves and molecular guidance cues.

Ephrin-As and early retinal waves are also required for the mapping of retinal axons to their subcortical targets, including eye-specific layers in the dLGN (Huberman et al., 2005; Muir-Robinson et al., 2002; Penn et al., 1998; Pfeiffenberger et al., 2005; Rossi et al., 2001; Torborg et al., 2005) and retinotopic map formation in the dLGN (Feldheim et al., 1998; Grubb et al., 2003) and superior colliculus (SC) (Chandrasekaran et al., 2005; Feldheim et al., 2000; McLaughlin et al., 2003; Mrsic-Flogel et al., 2005). Recent anatomical studies of these subcortical maps in mice deficient in both ephrin-A signaling and early retinal waves also indicated that these two pathways act together to guide the formation of eye-specific layers in the dLGN (Pfeiffenberger et al., 2005) and of retinotopic maps in the dLGN and SC (Pfeiffenberger et al., 2006). These studies raise the possibility that the functional deficit in cortex is simply due to aberrant topography in the retinal input to the dLGN. The measured sizes and positions of RFs of single neurons recorded in the dLGN and visual cortex rule out this possibility. Our computational model of cortical RFs as a sum of Gaussian geniculate RFs demonstrates that the degree of scatter in geniculate topography simply cannot account for the enlarged azimuthal receptive fields we see in cortex and that another 17° of scatter in cortical inputs is needed. This oversimplified model provides a lower bound to the disruption of geniculocortical mapping, as any non-Gaussian structure in receptive fields, or "proofreading" by plasticity mechanisms, would tend to counteract this scatter. Our quantitative comparisons of topography and RF structure in dLGN and cortex also confirm that the lack of organization seen in retrograde tracing of connections from dLGN to cortex actually represents further map disruption

rather than a compensatory process to correct the aberrant topography in the dLGN.

Elevation Is Specified by Distinct Mechanisms from Azimuth

The nearly complete disruption of azimuthal structure in the visual cortex of the ephrin-A2A5-β2 combination KOs contrasts with the preservation of near normal topography and receptive field size in the elevation axis. This finding establishes that the mechanisms responsible for organizing the azimuth and elevation axes are distinct. We have previously shown that the precision of the cortical elevation map is also reduced functionally in the $\beta2^{-/-}$ mouse, but the abnormality is very much less than that along the azimuth axis (Cang et al., 2005b), similar to the mapping of subcortical areas (Chandrasekaran et al., 2005; Grubb et al., 2003; McLaughlin et al., 2003). In the present case, the azimuthal defect is so dramatic that any interaction between the mechanisms responsible for the two axes of the map should be detectable as a disruption of the elevation map. This finding is especially surprising because the disruption in azimuthal organization by itself necessarily disrupts nearest-neighbor information, impairing the local correlation structure that could have played a role in both axes.

Our results also provide an answer to a long-standing question of systems neuroscience: what is the natural coordinate system for the visual field? From a theoretical perspective, polar coordinates (eccentricity and angle) may seem appropriate for describing position on a circular visual field, and polar coordinates are indeed used in studies of the human visual system. However, the fact that we can genetically uncouple the mapping of azimuth and elevation, the two Cartesian axes, indicates that these are in fact the natural axes of the visual system, at least for its development.

Given that early retinal waves are thought generally to be isotropic (Wong, 1999), it remains a mystery why patterned activity has a differential effect on topographic mapping along these two axes. Furthermore, the molecular mechanism underlying mapping the elevation axis of the retina is not understood as well as that of the azimuth axis. Anatomical studies of retinocollicular mapping have suggested that EphB-ephrinB and Wnt-Ryk signaling participate in the mapping of retinal axons along the dorsoventral axis (Hindges et al., 2002; Mann et al., 2002; Schmitt et al., 2006), but the roles of these signaling pathways in retinogeniculate or geniculocortical mapping or their interactions with early retinal waves have not been tested. Future studies that analyze functional organization will help determine whether they are responsible for the elevation map in the cortex.

Remnant Maps in Ephrin-A2A5-β2 Combination KOs

To our surprise, we found that, despite the massive scatter evident anatomically and in functional assays, a remnant map of azimuth in the visual cortex of the ephrin-A2A5-β2 combination KOs is revealed by using short bars for intrinsic signal imaging and by single- and multi-unit recordings to map receptive fields. What, then, accounts for the remnant functional map in V1 of these animals? One obvious candidate is ephrin-A3. Ephrin-A2, -A3, and -A5 account for almost all ephrin-A expression in the developing visual thalamus and cortex. Although ephrin-A3 is expressed only at low levels and not in obvious gradients in the developing visual system (Cang et al., 2005a; Feldheim et al., 1998; Pfeiffenberger et al., 2005), it has been demonstrated to contribute importantly to the establishment of topographic maps throughout the visual system, as ephrin-A2/A3/A5 triple KO mice have greater errors than ephrin-A2/A5 double KOs in the mapping of retinogeniculate, retinocollicular (Pfeiffenberger et al., 2006), and geniculocortical projections (see Figures 5D and 2 of Cang et al., 2005a, and compare with Figure 1A of current study). We were unable to create mice that lack all of ephrin-A2/A3/A5 and β2 because ephrin-A3 and β2 are genetically linked. It is conceivable that the azimuth map in such a quadruple KO would be completely abolished.

Another possibility is that factors other than the remnant ephrin-A3 signaling, such as other molecular guidance cues, timing of axonal ingrowth, or later activity-dependent refinement, could also be important for topographic mapping. Interestingly, the retrograde labeling pattern of geniculocortical projections in the combination KOs seemed to demonstrate a complete loss of topography, because two injections separated by nearly half the width of the visual cortex labeled completely overlapping groups of geniculate neurons (Figure 3), although these mice still have a remnant functional azimuth map. While it is possible that labeling with injections further apart in the cortex could reveal a remnant anatomical topography, the difference between anatomical and functional maps suggests that some process of synaptic refinement may account for the remnant functional maps in the combination KOs. Late-stage retinal waves (which are β2 independent) or visual experience (Smith and Trachtenberg, 2007) could participate in this process, which might operate similarly to the activity-dependent map refinement driven by early retinal waves. In the case of combination KOs, late functional refinement may be enhanced because the widespread anatomical inputs permit functional rearrangement without extensive growth to form new connections, perhaps merely by changes in the efficacy of existing connections. Consistent with this hypothesis, it has been shown that later spontaneous activity, around eye opening, plays a role in retinogeniculate refinement (Hooks and Chen, 2006). Such mechanisms could be capable of selecting the proper synaptic inputs even in the absence of a topographic anatomical projection and thus generating the rough functional map we observed.

Selective Disruption of Spatial Structure of Cortical Receptive Fields

Perturbations that affect axon pathfinding and synaptic connectivity could have varied effects on individual receptive fields, as illustrated in Figure 8. When the afferents are scrambled, downstream neurons may still be able to select the correct inputs through synaptic specificity or plasticity mechanisms, thereby proofreading and establishing a normal topographic output (top). Alternatively, they may be able to restrict their inputs to a small region of visual space, generating receptive fields of the appropriate size but in the wrong topographic location (middle). A third possibility is that target neurons may not perform any selection among the scrambled inputs, which would result in distorted receptive fields and scattered topography (bottom).

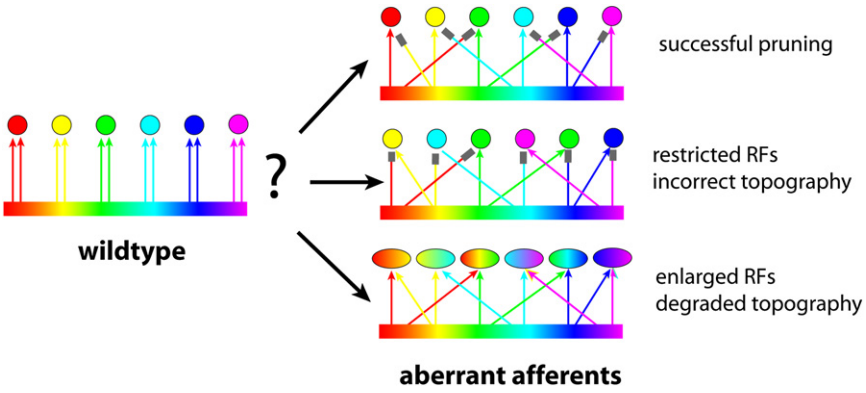

Figure 8. Hypotheses for Possible Consequences of Disrupting Afferent Organization in a Topographic Projection, Illustrating Differential Effects on Large-Scale Organization versus Local Receptive Field Structure

Previous studies, which have measured the effect of developmental mechanisms by anatomical tracing or imaging of topographic maps, could not distinguish among these possibilities, Here, using single-unit electrophysiology, we were able to investigate RF structures of individual neurons and found that cortical RFs were elongated almost 2-fold in the azimuth direction. Thus, perturbing ephrin-As and early activity results in defects both in large-scale map formation and in local receptive field structure, as in the third possibility cartooned in Figure 8.

The cortical result is in contrast to the deficit in dLGN, which follows the second scenario of Figure 8. In this case, the RF size and shape were generally maintained, but the topographic distribution was highly disrupted. A likely explanation for the difference between dLGN and cortex is that the convergence of synaptic inputs differs between the two visual areas. Relatively few retinal axons synapse onto a given dLGN neuron—recent data suggest inputs from ten or more retinal ganglion cells early in development are pruned down to just one to three strong inputs at maturity (Chen and Regehr, 2000; Jaubert-Miazza et al., 2005). Initial pruning has been shown to be dependent on spontaneous activity and thus may simply represent an extremely strong competitive plasticity mechanism that only retains the very most correlated inputs, i.e., those from a single retinal ganglion cell (whose axonal branches have perfectly correlated activity) or from a few neighboring ganglion cells with overlapping RFs. Final pruning takes place around eye opening (Hooks and Chen, 2006), after initial ingrowth and when ACh-dependent retinal waves are no longer present, and would therefore be expected to remain intact in the combination KOs. In contrast, cortical neurons in the input layer of cortex, layer IV, normally receive feedforward synapses from many dLGN cells. Although estimates of this number vary widely (Alonso et al., 2001; Bruno and Sakmann, 2006), it is at least an order of magnitude greater than retinogeniculate convergence. Also, because cortical RFs are larger than dLGN RFs, there is inherently less strict topographic correlation in cortical inputs. These two factors may combine to prevent cortical neurons from restricting their spatial structure to a normal extent when the topography of thalamocortical afferents is disrupted, as in the combination KO. The fact that the nature of individual RF defects in thalamus and cortex is consistent with these aspects of normal connectivity suggests that, even in the absence of long-range topographic information, neurons may follow normal developmental rules in establishing connectivity, simply using disrupted upstream information.

Interestingly, despite the distortion in the extents of individual cortical RFs, their centers still display signs of topographic organization. Part of this is likely due to the law of large numbers—even if the inputs are widespread, summing over a large number of inputs will reveal order in their centroids if there is any weak organization at all. It also suggests that perhaps topographic organization is a very robust state and that even the weak patterning generated by the remnant ephrin-A3 or late patterned activity is enough to break symmetry and lead to at least a rough map.

In summary, the defects in both local receptive field structure and global map topography in the combination KOs, as revealed by a combination of anatomy, functional imaging, and extracellular recording, demonstrate a key role of ephrin-As and early retinal waves as distinct pathways in the development of connectivity in the visual system, which together account almost completely for the formation of a functional azimuth map. The dramatic decoupling between the azimuth and elevation axes demonstrates that spatial information in the developing brain is organized along two independent Cartesian axes. While it is likely that all CNS projections that are mapped topographically will use a combination of ephrins or similar molecular cues and neural activity for their development, the relative importance of each may vary between brain structures. Similar experiments in other regions of the nervous system will reveal the generality of these mechanisms.

EXPERIMENTAL PROCEDURES

Animals

To determine the consequences for cortical retinotopic maps and RFs of simultaneously removing ephrin-A ligands and disrupting early retinal waves, we crossed mice lacking the β2 subunit of nicotinic acetylcholine receptor ($\beta2^{-/-}$) (Cang et al., 2005b; Xu et al., 1999) with those deficient for ephrin-A ligands (Cang et al., 2005a; Feldheim et al., 2000; Pfeiffenberger et al., 2005) to obtain ephrin-A2A5-β2 combination KOs ($A2^{-/-}/A5^{-/-}$-$\beta2^{-/-}$) (Pfeiffenberger et al., 2006). Their littermates and additional mice with same genetic background were used as controls, including $A2^{-/-}A5^{-/-}\beta2^{+/\pm}$, $A2^{+/\pm}A5^{+/-}\beta2^{-/-}$. The WT controls for optical imaging (Figure 1) and retrograde tracing (Figure 3) were obtained from reanalyzing some of the WT mice included in our previous study (Cang et al., 2005b). For receptive field mapping in the lateral geniculate nuclei, WT mice from the C57Bl/6 strain were used as controls.

The animals were maintained in the animal facility at UC Santa Cruz, UC San Francisco, or Northwestern University and used in accordance with protocols approved by the UCSC, UCSF, and Northwestern University Institutional Animal Care and Use Committee. Ephrin-A2, -A3, -A5, and β2 mutations were genotyped as previously described (Cutforth et al., 2003; Feldheim et al., 2000; Frisén et al., 1998; Xu et al., 1999).

Retrograde Labeling of Thalamocortical Projections and Image Analysis

Cholera toxin subunit B (CTB) conjugated to Alexa Fluor (Molecular Probes, OR), CTB-488 (green), and CTB-594 (red) were injected into the cortex to retrogradely label dLGN neurons, at about 500 μm apart along either the azimuth or elevation axis (Cang et al., 2005a, 2005b). A small amount of 2 mg/ml solution of each CTB in PBS was injected by Nanoject (Drummond Scientific Company, PA) using a glass pipette with 20–30 μm tip opening, with injection volume of 32.2 nl. Mice were sacrificed and intracardially perfused with 4% paraformaldehyde in PBS 48 hr later. The brains were fixed overnight before sectioning at 100 μm coronally using a vibratome (Lancer, MO) or a vibroslice 752M (Campden Instruments Ltd, Lafayette, IN). Images of the dLGN and injection sites in the cortex were captured with a confocal microscope (Biorad MRC 1024, CA, or Zeiss LSM5 Pascal, Germany).

To analyze the separation of retrogradely labeled cells of the two colors in the dLGN, we first calculated the background signal as the mean signal of an area within the dLGN where no labeled cells were seen. The image was then thresholded separately for each color at the level of 1.5 time the background. Similar results were obtained with thresholds of 1.4, 1.6, and 1.7. We then calculated the position of the center of mass for all the labeled pixels (weighted by intensity) within the dLGN. The distribution of labeled pixels of each color (with each suprathreshold pixel given equal weight) was plotted along the line connecting the two centers and was then analyzed to quantify the overlap of the two groups of labeled cells. We determined an "overlap index" by calculating the inverse of the distance between the distributions of the two colors in the unit of their standard deviations, i.e., overlap index = sqrt(Variance of first distribution/2 + Variance of second distribution/2)/distance. The above procedure was performed for one representative section of every animal, usually the third or fourth of six to seven 100 μm sections of the dLGN.

Functional Imaging and Analysis of Retinotopic Maps

Retinotopic maps in the mouse visual cortex were imaged and analyzed according to our published protocols (Cang et al., 2005a, 2005b; Kalatsky and Stryker, 2003). In brief, adult mice (2- to 6-month-old) were anesthetized with urethane (1.0 g/kg in 10% saline solution). Optical images of the cortical intrinsic signal were obtained at the wavelength of 610 nm using Dalsa 1M30 CCD camera (Dalsa, Waterloo, Canada) controlled by custom software. A high refresh rate monitor (Nokia Multigraph 445X, 1024 × 768 pixel @ 120 Hz) was placed 25 cm away from the animal. Drifting thin bars (2° wide and full screen long) were generated by a Matrox G450 board (Matrox Graphics, Inc., Quebec, Canada) and displayed on the monitor. Animals were presented with thin bars drifting along the dorsoventral or nasotemporal axis in order to stimulate the constant lines of elevation or azimuth, respectively. By extracting the optical signal at the stimulus frequency, we computed the response magnitudes and timing in reference to the stimulus cycle, which can then be converted to the location of visual field. The absolute phase maps were then calculated by the method of "phase reversal" (Kalatsky and Stryker, 2003). 0° phase indicates the midline of the monitor, both horizontally and vertically.

To assess map quality, we analyzed the phase scatter of the retinotopic maps. Specifically, we used the elevation map to select the response area, because the azimuth maps of the mutant mice were weak and more defective. The 20,000 pixels (1.60 mm^2 of cortical space) that have the greatest response magnitude in the elevation maps were selected. For each of these pixels, we calculated the difference between its phase value and the mean phase value of its surrounding 25 pixels. For maps of high quality, the phase differences are quite small because of smooth phase progression. The standard deviation of the phase difference was then used as an index of map quality.

In addition, spatially restricted stimuli were used to assay the disruption of azimuth map. Short horizontal bars of 20° long and 2° wide drifted vertically along different azimuthal positions on the monitor. Retinotopic maps in response to these stimuli were obtained using the same method as those using full-screen bars. To study the profile of response magnitude to the restricted stimuli, we determined the areas activated by full-screen horizontal bars and short bars along the center of the video monitor (0° phase, horizontally), respectively (thresholded by 50% of peak response). A ratio between these areas was calculated (Figure 3G) to quantify the disruption of the azimuth map.

Extracellular Recording of Cortical and Geniculate Receptive Fields

We performed multisite extracellular recordings in V1, using silicon microprobes from NeuroNexusTechnologies (Ann Arbor, MI). Electrodes with 16 sites, spaced at 50 μm, were inserted radially ~800–1000 μm into cortex, allowing us to record simultaneously from all layers. For recording from the dLGN, we used 10 MΩ tungsten electrodes (Frederick Haer Company, Bowdoinham, ME). Electrodes were inserted at 2.2 mm lateral and 2.8 mm posterior from the bregma suture. At a depth of ~2500–3000 μm, the dLGN could be identified by rapid firing in response to either ON or OFF flashes of a small spot at a specific location in the visual field. In both cases, signals were acquired using a System 3 workstation (Tucker Davis Technologies, FL) and analyzed with custom software in Matlab. To separate single units, spike waveforms were characterized with the first four principal components and clustered with KlustaKwik (Harris et al., 2000). Quality of separation was determined based on the Mahalanobis distance and L-ratio (Schmitzer-Torbert et al., 2005).

Stimuli were generated in Matlab using the Psychophysics Toolbox extensions (Brainard, 1997; Pelli, 1997). To map receptive fields in cortex, short white bars, 5° wide and 10° long, were swept across the visual field at 25°/s at different horizontal and vertical positions. For sweeps at each position, the spikes were binned at 400 ms intervals, corresponding to motion across 10° of visual space. The receptive field was then constructed using position of the sweep along one axis and spike timing along the other axis. These receptive fields were fit to a two-dimensional Gaussian, giving a receptive field center and radius in both azimuth and elevation. The process was repeated for both horizontal and vertical sweeps. Since many cells respond more strongly to one orientation, the final RF parameters were calculated by weighting the average of the parameters from the two directions by the amplitude of the corresponding Gaussian fit. Receptive fields were linearly interpolated to give smooth images for figures. To measure dLGN receptive fields, a similar process was used, except that stimuli consisted of light or dark squares 10° across, flashed for 200 ms at random locations on a grid with 10° spacing. For multisite cortical recordings, the scatter of receptive field positions for a given radial penetration was determined by taking the standard deviation of receptive field center for all multi-units recorded during that penetration.

Receptive Field Simulation

A simple model of cortical receptive field structure was constructed in Matlab. Individual geniculate RFs were generated as Gaussians with a width given by the average experimentally measured RF size and a center displaced from its nominal location by a random value drawn from a normal distribution with width given by the average experimentally measured map scatter. An individual cortical receptive field was generated by pooling N (1 to 50) such geniculate RFs, with nominal centers drawn from a normal distribution appropriate to generate the average control cortical receptive field. The size of the cortical RF was measured by summing all N geniculate RFs and taking the standard deviation of the resulting distribution. This process was repeated 500 times to determine the average cortical RF size. The standard deviation of the resulting RF positions was used as the measure of cortical RF scatter. Additional geniculocortical scatter was modeled by jittering the centers of the geniculate RFs by an additional amount drawn from normal distributions of different widths in order to determine the amount of additional scatter necessary to match experimental data. The model was not strongly dependent on the assumption of linear summation; passing the summed response through either a quadratic or square-root nonlinearity changed the parameters that fit the WT data, but still left a highly significant gap ($p < 0.01$) between the predicted and observed size of combination knockout RFs.

SUPPLEMENTAL DATA

The Supplemental Data for this article can be found online at http://www.neuron.org/cgi/content/full/57/4/511/DC1/.

ACKNOWLEDGMENTS

The work was supported by US National Institutes of Health (NIH) grants EY014689 (D.A.F.) and EY02874 (M.P.S.). J.C. was an Aventis

Pharmaceuticals Fellow of the Life Sciences Research Foundation, and C.M.N. is a Helen Hay Whitney Foundation Fellow. We thank members of the Feldheim and Stryker labs for thoughtful discussion, Dr. Tom Bozza for the use of a confocal microscope, and Dr. David Ferster for the use of a Vibratome.

Received: March 29, 2007
Revised: October 31, 2007
Accepted: December 19, 2007
Published: February 27, 2008

REFERENCES

Alonso, J.M., Usrey, W.M., and Reid, R.C. (2001). Rules of connectivity between geniculate cells and simple cells in cat primary visual cortex. J. Neurosci. *21*, 4002–4015.

Brainard, D.H. (1997). The psychophysics toolbox. Spat. Vis. *10*, 433–436.

Bruno, R.M., and Sakmann, B. (2006). Cortex is driven by weak but synchronously active thalamocortical synapses. Science *312*, 1622–1627.

Cang, J., Kaneko, M., Yamada, J., Woods, G., Stryker, M.P., and Feldheim, D.A. (2005a). Ephrin-as guide the formation of functional maps in the visual cortex. Neuron *48*, 577–589.

Cang, J., Renteria, R.C., Kaneko, M., Liu, X., Copenhagen, D.R., and Stryker, M.P. (2005b). Development of precise maps in visual cortex requires patterned spontaneous activity in the retina. Neuron *48*, 797–809.

Chandrasekaran, A.R., Plas, D.T., Gonzalez, E., and Crair, M.C. (2005). Evidence for an instructive role of retinal activity in retinotopic map refinement in the superior colliculus of the mouse. J. Neurosci. *25*, 6929–6938.

Chandrasekaran, A.R., Shah, R.D., and Crair, M.C. (2007). Developmental homeostasis of mouse retinocollicular synapses. J. Neurosci. *27*, 1746–1755.

Chen, C., and Regehr, W.G. (2000). Developmental remodeling of the retinogeniculate synapse. Neuron *28*, 955–966.

Chklovskii, D.B., and Koulakov, A.A. (2004). Maps in the brain: what can we learn from them? Annu. Rev. Neurosci. *27*, 369–392.

Cline, H. (2003). Sperry and Hebb: oil and vinegar? Trends Neurosci. *26*, 655–661.

Cutforth, T., Moring, L., Mendelsohn, M., Nemes, A., Shah, N.M., Kim, M.M., Frisen, J., and Axel, R. (2003). Axonal ephrin-As and odorant receptors: coordinate determination of the olfactory sensory map. Cell *114*, 311–322.

Feldheim, D.A., Vanderhaeghen, P., Hansen, M.J., Frisen, J., Lu, Q., Barbacid, M., and Flanagan, J.G. (1998). Topographic guidance labels in a sensory projection to the forebrain. Neuron *21*, 1303–1313.

Feldheim, D.A., Kim, Y.I., Bergemann, A.D., Frisen, J., Barbacid, M., and Flanagan, J.G. (2000). Genetic analysis of ephrin-A2 and ephrin-A5 shows their requirement in multiple aspects of retinocollicular mapping. Neuron *25*, 563–574.

Flanagan, J.G. (2006). Neural map specification by gradients. Curr. Opin. Neurobiol. *16*, 59–66.

Flanagan, J.G., and Vanderhaeghen, P. (1998). The ephrins and Eph receptors in neural development. Annu. Rev. Neurosci. *21*, 309–345.

Frisén, J., Yates, P.A., McLaughlin, T., Friedman, G.C., O'Leary, D.D.M., and Barbacid, M. (1998). Ephrin-A5 (AL-1/RAGS) is essential for proper retinal axon guidance and topographic mapping in the mammalian visual system. Neuron *20*, 235–243.

Grubb, M.S., and Thompson, I.D. (2003). Quantitative characterization of visual response properties in the mouse dorsal lateral geniculate nucleus. J. Neurophysiol. *90*, 3594–3607.

Grubb, M.S., Rossi, F.M., Changeux, J.P., and Thompson, I.D. (2003). Abnormal functional organization in the dorsal lateral geniculate nucleus of mice lacking the beta 2 subunit of the nicotinic acetylcholine receptor. Neuron *40*, 1161–1172.

Hanson, M.G., and Landmesser, L.T. (2004). Normal patterns of spontaneous activity are required for correct motor axon guidance and the expression of specific guidance molecules. Neuron *43*, 687–701.

Harris, K.D., Henze, D.A., Csicsvari, J., Hirase, H., and Buzsaki, G. (2000). Accuracy of tetrode spike separation as determined by simultaneous intracellular and extracellular measurements. J. Neurophysiol. *84*, 401–414.

Hindges, R., McLaughlin, T., Genoud, N., Henkemeyer, M., and O'Leary, D.D. (2002). EphB forward signaling controls directional branch extension and arborization required for dorsal-ventral retinotopic mapping. Neuron *35*, 475–487.

Hooks, B.M., and Chen, C. (2006). Distinct roles for spontaneous and visual activity in remodeling of the retinogeniculate synapse. Neuron *52*, 281–291.

Huberman, A.D., Murray, K.D., Warland, D.K., Feldheim, D.A., and Chapman, B. (2005). Ephrin-As mediate targeting of eye-specific projections to the lateral geniculate nucleus. Nat. Neurosci. *8*, 1013–1021.

Jaubert-Miazza, L., Green, E., Lo, F.S., Bui, K., Mills, J., and Guido, W. (2005). Structural and functional composition of the developing retinogeniculate pathway in the mouse. Vis. Neurosci. *22*, 661–676.

Kalatsky, V.A., and Stryker, M.P. (2003). New paradigm for optical imaging: temporally encoded maps of intrinsic signal. Neuron *38*, 529–545.

Mann, F., Ray, S., Harris, W., and Holt, C. (2002). Topographic mapping in dorsoventral axis of the Xenopus retinotectal system depends on signaling through ephrin-B ligands. Neuron *35*, 461–473.

McLaughlin, T., and O'Leary, D.D. (2005). Molecular gradients and development of retinotopic maps. Annu. Rev. Neurosci. *28*, 327–355.

McLaughlin, T., Torborg, C.L., Feller, M.B., and O'Leary, D.D. (2003). Retinotopic map refinement requires spontaneous retinal waves during a brief critical period of development. Neuron *40*, 1147–1160.

Mrsic-Flogel, T.D., Hofer, S.B., Creutzfeldt, C., Cloez-Tayarani, I., Changeux, J.P., Bonhoeffer, T., and Hubener, M. (2005). Altered map of visual space in the superior colliculus of mice lacking early retinal waves. J. Neurosci. *25*, 6921–6928.

Muir-Robinson, G., Hwang, B.J., and Feller, M.B. (2002). Retinogeniculate axons undergo eye-specific segregation in the absence of eye-specific layers. J. Neurosci. *22*, 5259–5264.

Nicol, X., Voyatzis, S., Muzerelle, A., Narboux-Neme, N., Sudhof, T.C., Miles, R., and Gaspar, P. (2007). cAMP oscillations and retinal activity are permissive for ephrin signaling during the establishment of the retinotopic map. Nat. Neurosci. *10*, 340–347.

O'Leary, D.D.M., and Wilkinson, D.G. (1999). Eph receptors and ephrins in neural development. Curr. Opin. Neurobiol. *9*, 65–73.

O'Leary, D.D., and McLaughlin, T. (2005). Mechanisms of retinotopic map development: Ephs, ephrins, and spontaneous correlated retinal activity. Prog. Brain Res. *147*, 43–65.

Pelli, D.G. (1997). The VideoToolbox software for visual psychophysics: transforming numbers into movies. Spat. Vis. *10*, 437–442.

Penn, A.A., Riquelme, P.A., Feller, M.B., and Shatz, C.J. (1998). Competition in retinogeniculate patterning driven by spontaneous activity. Science *279*, 2108–2112.

Pfeiffenberger, C., Cutforth, T., Woods, G., Yamada, J., Renteria, R.C., Copenhagen, D.R., Flanagan, J.G., and Feldheim, D.A. (2005). A combination of ephrinAs and neural activity are required for patterning eye-specific layers during retinogeniculate mapping. Nat. Neurosci. *8*, 1022–1027.

Pfeiffenberger, C., Yamada, J., and Feldheim, D.A. (2006). Ephrin-As and patterned retinal activity act together in the development of topographic maps in the primary visual system. J. Neurosci. *26*, 12873–12884.

Rossi, F.M., Pizzorusso, T., Porciatti, V., Marubio, L.M., Maffei, L., and Changeux, J.P. (2001). Requirement of the nicotinic acetylcholine receptor beta 2 subunit for the anatomical and functional development of the visual system. Proc. Natl. Acad. Sci. USA *98*, 6453–6458.

Schmitt, A.M., Shi, J., Wolf, A.M., Lu, C.C., King, L.A., and Zou, Y. (2006). Wnt-Ryk signalling mediates medial-lateral retinotectal topographic mapping. Nature *439*, 31–37.

Schmitzer-Torbert, N., Jackson, J., Henze, D., Harris, K., and Redish, A.D. (2005). Quantitative measures of cluster quality for use in extracellular recordings. Neuroscience *131*, 1–11.

Smith, S.L., and Trachtenberg, J.T. (2007). Experience-dependent binocular competition in the visual cortex begins at eye opening. Nat. Neurosci. *10*, 370–375.

Torborg, C.L., and Feller, M.B. (2005). Spontaneous patterned retinal activity and the refinement of retinal projections. Prog. Neurobiol. *76*, 213–235.

Torborg, C.L., Hansen, K.A., and Feller, M.B. (2005). High frequency, synchronized bursting drives eye-specific segregation of retinogeniculate projections. Nat. Neurosci. *8*, 72–78.

Tsigankov, D.N., and Koulakov, A.A. (2006). A unifying model for activity-dependent and activity-independent mechanisms predicts complete structure of topographic maps in ephrin-A deficient mice. J. Comput. Neurosci. *21*, 101–114.

Wong, R.O. (1999). Retinal waves and visual system development. Annu. Rev. Neurosci. *22*, 29–47.

Xu, Q., Mellitzer, G., Robinson, V., and Wilkinson, D.G. (1999). In vivo cell sorting in complementary segmental domains mediated by Eph receptors and ephrins. Nature *399*, 267–271.